A NUMERICAL EXAMINATION OF AN UNSTEADY NONLINEAR MHD FLOW IN THE PRESENCE OF THERMAL RADIATION AND HEAT GENERATION

T.M. AGBAJE* and P.G.L. LEACH

Institute of Systems Science, Durban University of Technology P O Box 1334
Durban 4000, SOUTH AFRICA
E-mail: titilayoagbaje@gmail.com

In this study, the spectral perturbation method and the spectral relaxation method are used to solve the nonlinear differential equations of an unsteady nonlinear MHD flow in the presence of thermal radiation and heat generation. The SPM is mainly based on series expansion, generating series approximation coupled with the Chebyshev spectral method. The numerical results generated using the spectral perturbation method were compared with those found in the literature, and the two results were in good agreement.

Key words: unsteady MHD flow, spectral perturbation method, spectral relaxation method, thermal radiation, heat generation.

1. Introduction

The investigations of boundary layer flow and heat transfer problems due to a stretching sheet have attracted much attention of researchers due to their applications in various engineering and manufacturing processes [1-3]. Such engineering applications include cooling of metallic sheets and aerodynamic extrusion of plastic sheets. In addition, applications in manufacturing processes occur in glass blowing, metal extrusion, the spinning of metal, fiber spinning, continuous casting, and constant stretching of plastic films. Magneto-hydrodynamics (MHD) flow also plays a crucial role in the metallurgical process, such as annealing, drawing, and copper wire thinning. Literature surveys show that many researchers have shifted their attention towards unsteady flows because their solutions often give a more explicit physical meaning of the problem. The equations that will be examined in this study are obtained by considering unsteady nonlinear MHD flow in the presence of thermal radiation and heat generation. Radiative heat transfer plays a very crucial role in gas turbines and various propulsion devices for aircraft, manufacturing industries for the design of reliable equipment, space vehicles, missiles, and satellites. Based on these applications, Olanrewaju *et al.* [4] investigated numerically an unsteady three-dimensional MHD flow and mass transfer in the presence of thermal radiation using the sixth-order Runge-Kutta-Fehlberg method with shooting technique. Olanrewaju and Makinde [5] investigated unsteady convection with chemical reaction and radiative heat transfer past a flat porous plate moving through a binary mixture using the fourth-order Runge-Kutta integration scheme along with shooting technique. Abbas *et al*. [6] dealt with the effects of radiation and magnetic field on the mixed convection stagnation-point flow over a vertical stretching sheet in a porous medium. The series solutions of the coupled nonlinear system are obtained using an analytical technique, namely the homotopy analysis method (HAM). A considerable amount of literature now exists that employed the perturbation series approach in the solution of unsteady flows. These investigations include the study of Seshadri *et al.* [7] who used the perturbation series approach for the solution of an unsteady mixed convection flow along a heated vertical plate. Nazar *et al*. [8] used the perturbation series approach to obtain first-order perturbation approximation of the solution of an unsteady boundary layer flow due to a stretching surface in a rotating fluid. Liao [9] observed the limitation of the perturbation series approach used in [7,8], i.e. the perturbation solutions are valid only for

a minimal time. An analytical approach used as an alternative approach to address some of the limitations of the perturbation method was proposed by Liao [9]. The approach is based on the homotopy analysis method (HAM) and gives results that are uniformly valid for all time. Many researchers have ever since then adopted the method in solving unsteady flow problems. These include Kumari and Nath [2], Hayat *et al*. [3], Liao [9], Mehmood *et al*. [10], Xu *et al*. [11], etc. According to Liao [9], one attractive advantage of the homotopy analysis method (HAM) over the standard perturbation method for the solution of unsteady boundary layer flow problems is that the (HAM) provides flexibility in the choice of initial approximation and linear operator which can be carefully chosen so that the higher-order approximation can be integrated analytically. This HAM advantage contradicts the conclusion earlier drawn by researchers about the perturbation methods that analytical solution cannot be obtained beyond first-order approximation for higher-order perturbation equations in unsteady flow problems. In the application of the HAM technique, the nonlinear PDEs describing the unsteady flow problems are reduced to an infinite number of linear ordinary differential equations that are governed by an auxiliary linear operator that can be used to control the convergence of the solution. The primary aim of this study is to extend the analysis of Awad *et al*. [12] by introducing the thermal radiation and heat generation effect. This is because of the important space technology and processes involving high temperatures. The test equations will be solved using the spectral perturbation method (SPM) and spectral relaxation method (SRM). The use and accuracy of the SPM have been demonstrated for the solution of MHD stagnation point flow and heat transfer towards a stretching sheet and unsteady two-dimensional boundary layer flow problem. It was shown in previous research that the SPM could be used as an alternative numerical approach for solving both nonlinear ODEs and PDEs. The SPM combines the use of the standard perturbation approach with the Chebyshev pseudo-spectral method to generate a numerical solution of higher-order perturbation equations describing the flow not possible to solve analytically. With the SPM, solutions to partial differential equations can be obtained by applying discretization only in the space direction. Applying discretization only in the space direction and integrating using the Chebyshev spectral collocation method makes the SPM computationally efficient. The Chebyshev pseudo-spectral method is used because of its high-level accuracy. Also, using spectral methods, only a few grid points are required to yield accurate results. Using the spectral method to integrate the perturbation equations, very accurate solutions that are valid for all time domains are obtained. Numerical simulations on the equations are conducted using the spectral perturbation method (SPM). Results generated using the spectral perturbation method SPM are compared and validated with the published work of Awad *et al*. [12], who used the spectral quasilinearisation method (SQLM) and the spectral homotopy analysis method (SHAM), and the methods show good agreement. A sizeable amount of literature now exists based on the use of the SPM for the solution of fluid mechanics based ordinary differential equations (ODEs) and partial differential equations (PDEs) problems, (see for example, Agbaje and Motsa, [13]; Motsa [14]; Agbaje *et al*. [15]; [16]. The results obtained show that the SPM can be used efficiently to solve systems of partial differential equations principally those defined under the William and Rhyne [17] transformation.

In this work, we investigate unsteady nonlinear MHD flow in the presence of thermal radiation described by systems of partial differential equations PDEs. The accuracy of the method was shown by validating the SPM results against the results obtained from the literature, and the results were found to be in good agreement. The study also sought to investigate the accuracy and efficiency of the SPM. This present work, however, shows that accurate results can be obtained using the perturbation method.

2. Problem Formulation

According to Awad *et al*. [12], the unsteady nonlinear convection of a fluid over a stretching flat plate is investigated. Initially, $(t=0)$, both the fluid and stretching plate are kept at a constant temperature T_w and concentration C_∞ where $T_w > T_\infty$ correspond to the heated plate and $T_w < T_\infty$ is for a cooled plate. It is assumed that at $t=0$, the velocity of the stretching plate is $u_w = ax$, where a is a positive constant. From the Boussinesq approximation, density is related to the temperature and concentration by the equation

$$\rho = \rho_0 \left[1 - \beta_T (T - T_\infty) + \beta_C (C - C_\infty) \right]. \tag{2.1}$$

In the case of thermal stratification and heat released by viscous dissipation, wall jet like profiles induce significant changes in density gradients, and the density depends on the temperature or temperature and concentration in a nonlinear form:

$$\rho = \rho_\infty \left[1 - \beta_T (T - T_\infty) + \beta_I (T - T_\infty)^2 \right]. \tag{2.2}$$

The formulation below was used by Karcher and Müller [18] to define the nonlinearity of the relationship between the density, temperature and concentration:

$$\rho = \rho_\infty \left[1 - \beta_0 (T - T_\infty) - \beta_I (T - T_\infty)^2 - \beta_2 (C - C_\infty) \right] \tag{2.3}$$

where ρ_∞ is the constant fluid density, T_∞ and C_∞ are the fluid temperature and solutal concentration, respectively, ρ_0 and ρ_2 are the coefficients of the thermal and solutal expansion, and ρ_I connotes the nonlinear coefficient of thermal expansion. The natural nonlinear convection in a non-Darcy porous medium was investigated by Partha [19] using a temperature-concentration-dependent density relation in the form

$$\rho = \rho_0 \left[\beta_0 (T - T_\infty) - \beta_I (T - T_\infty)^2 - \beta_2 (C - C_\infty) + \beta_3 (C - C_\infty)^2 \right]. \tag{2.4}$$

With the usual Boussinesq and the boundary layer approximations, the governing equations are written in the form:

$$\frac{\partial u}{\partial x} + \frac{\partial v}{\partial y} = 0, \tag{2.5}$$

$$\frac{\partial u}{\partial t} + u\frac{\partial u}{\partial x} + v\frac{\partial u}{\partial y} = \nu\frac{\partial^2 u}{\partial y^2} + \left[\beta_0 (T - T_\infty) + \beta_I (T - T_\infty)^2 \right] + $$
$$+ \left[\beta_2 (C - C_\infty) + \beta_2 (C - C_\infty)^2 \right] g, \tag{2.6}$$

$$\frac{\partial T}{\partial t} + u\frac{\partial T}{\partial x} + v\frac{\partial T}{\partial y} = \alpha_m\frac{\partial^2 T}{\partial y^2} - \frac{1}{\rho C_p}\frac{\partial q_r}{\partial y} + \frac{Q_0}{\rho C_p}(T - T_\infty), \tag{2.7}$$

$$\frac{\partial C}{\partial t} + u\frac{\partial C}{\partial x} + v\frac{\partial C}{\partial y} = D\frac{\partial^2 C}{\partial y^2} \tag{2.8}$$

where t, u and v are the time, fluid tangential velocity and normal velocity components along the x and y directions, respectively, T and C are the local fluid temperature and local solute concentration across the boundary layer, respectively, g is the acceleration due to gravity, ρ is the fluid density, ν is the kinematic viscosity, $\alpha_m = \left(\dfrac{K_0}{\rho C_p} \right)$ is the thermal diffusivity with K_0 being the fluid thermal conductivity ratio and C_p

the specific heat at constant pressure of the fluid, Q_0 is the heat generation constant, D is the mass diffusivity, σ is the fluid electrical conductivity, β_0 and β_1 are the thermal expansion coefficients and β_2 and β_3 are the solutal expansion coefficients.

The appropriate initial conditions are written as

$$t < 0: \quad u = 0, \quad v = 0, \quad T = T_w, \quad C = C_w, \quad \forall x, y. \tag{2.9}$$

The boundary conditions are:

$$t \geq 0 : u = ax, \quad v = 0, \quad T = T_w \quad C = C_w, \quad \text{at} \quad y = 0,$$

$$t \geq 0 : u \to 0, \quad T \to T_\infty, \quad C \to C_\infty \quad \text{as} \quad y \to \infty, \tag{2.10}$$

where a, is a constant.

The stream function ψ is introduced and defined as:

$$u = \frac{\partial \psi}{\partial y}, \qquad v = -\frac{\partial \psi}{\partial x}. \tag{2.11}$$

Further, it is convenient to choose time scale ξ so that the region of the time integration can be finite. Such transformations have been introduced by Williams and Rhyne [17] in a related study. The transformations are expressed as

$$\xi = 1 - \exp(-\tau), \quad \tau = bt, \tag{2.12}$$

with b a positive constant and t is the time variable. The Williams and Rhyne's [17] transformations in Eq.(2.12) are used to convert it from the infinite (original) time scale $0 \leq \tau < \infty$ to the finite scale $0 \leq \xi \leq 1$ so that the interval of integration is collapsed from an infinite domain to a finite domain.

The similarity variables given in [12] is used and written below as

$$\eta = \sqrt{\frac{a}{v\xi}} y, \qquad \psi = \sqrt{av\xi} \, xf(\xi, \eta), \qquad \theta(\xi, \eta) = \frac{T - T_\infty}{T_w - T_\infty}, \qquad \phi(\xi, \eta) = \frac{C - C_\infty}{C_w - C_\infty}. \tag{2.13}$$

Equations (2.6)-(2.8) along with the boundary conditions (2.10) can be presented in the form:

$$f''' + \frac{\eta}{2}(1 - \xi)f'' + \xi\left[ff'' - (f')^2\right] +$$

$$+ \lambda\xi\left[(1 + \alpha\theta)\theta + N_b(1 + \sigma\phi)\phi\right] = \xi(1 - \xi)\frac{\partial f'}{\partial \xi}, \tag{2.14}$$

$$\left(1 + \frac{4N_R}{3}\right)\theta'' + \Pr(1 - \xi)\frac{\eta}{2}\theta' + \Pr\xi f\theta' + He\xi\theta = \Pr\xi(1 - \xi)\frac{\partial \theta}{\partial \xi}, \tag{2.15}$$

$$\frac{1}{Le}\phi'' + \frac{\eta}{2}Sc(1 - \xi)\phi' + Sc\xi f\phi' = Sc\xi(1 - \xi)\frac{\partial \phi}{\partial \xi}, \tag{2.16}$$

subject to the boundary conditions

$$f(\xi,0) = 0, \quad f'(\xi,0) = 1, \quad f'(\xi,\infty) = 0, \quad \theta(\xi,0) = 1,$$

$$\theta(\xi,\infty) = 0, \quad \phi(\xi,0) = 1, \quad \phi(\xi,\infty) = 0. \tag{2.17}$$

In the above equations, prime denotes the derivative with respect to η and the parameters are defined as

$$\mathrm{Ra}_x = \frac{\left(1 - \hat{\phi}_{f\infty}\right) g \beta_0 \rho f_\infty \Delta T x}{\alpha_m a}, \quad \gamma = \frac{\beta_1 \left(T_w - T_\infty\right)}{\beta_0}, \quad \sigma = \frac{\beta_3 \left(\hat{\phi}_w - \hat{\phi}_\infty\right)}{\beta_2},$$

$$N_b = \frac{\left(\rho_p - \rho_\infty\right)\left(\hat{\phi}_w - \hat{\phi}_\infty\right)}{\beta_0 \rho f \infty \left(1 - \hat{\phi}_\infty\right)\left(T_w - T_\infty\right)}, \quad \mathrm{Pr} = \frac{\nu}{\alpha_m}, \quad \mathrm{Sc} = \frac{\nu}{D_B}, \tag{2.18}$$

$$\mathrm{Le} = \frac{\alpha_m}{D_B}, \quad \mathrm{Pe}_x = \frac{u_w x}{\alpha_m}, \quad \lambda = \frac{\mathrm{Ra}_x}{Pe_x}, \quad N_R = \frac{16\sigma^* T_\infty^3}{3 k^* K_0}$$

where Ra_x is the Rayleigh number, γ is the nonlinear temperature parameter, N_b is the buoyancy parameter, N_R the thermal radiation parameter, Pr is Prandtl number, He the heat generation parameter, Sc is Schmidt number, Pe_x is the Peclet number, and Le the Lewis number. The skin friction and heat and mass transfer coefficients are described by the local skin friction coefficients, Nusselt number Nu, and the Sherwood number Sh defined as

$$\tau_w = \mu \frac{\partial u}{\partial y}\bigg|_{y=0}, \quad q_w = -\alpha_m \frac{\partial T}{\partial y}\bigg|_{y=0}, \quad q_m = -D\frac{\partial C}{\partial y}\bigg|_{y=0}. \tag{2.19}$$

The non-dimensionless form of the skin friction coefficient, the reduced Nusselt number, and the reduced Sherwood number are:

$$\xi^{\frac{1}{2}} \mathrm{Re}_x^{\frac{1}{2}} C_f = f''(\xi,0), \quad \xi^{\frac{1}{2}} \mathrm{Re}_x^{-\frac{1}{2}} \mathrm{Nu} = -\theta'(\xi,0), \quad \xi^{1/2} \mathrm{Re}_x^{-1/2} \mathrm{Sh} = -\phi'(\xi,0). \tag{2.20}$$

For the initial unsteady state flow, when $\xi = 0$, corresponding to $\tau = 0$, Eqs (2.14)-(2.16) become:

$$f''' + \frac{\eta}{2} f'' = 0, \quad \left(1 + \frac{4 N_R}{3}\right)\theta'' + \mathrm{Pr}\frac{\eta}{2}\theta' = 0, \quad \frac{1}{\mathrm{Le}}\phi'' + \mathrm{Sc}\frac{\eta}{2}\phi' = 0, \tag{2.21}$$

subject to the boundary conditions,

$$f(0) = 0, \quad f'(0) = 1, \quad f'(\infty) = 0, \quad \theta(0) = 1,$$

(2.22)

$$\theta(\infty) = 0, \quad \phi(0) = 1, \quad \phi(\infty) = 0.$$

Equations (2.21) alongside with the boundary conditions (2.24) admit closed form analytical solutions of the form:

$$f(0,\eta) = \eta\, \text{erfc}\left(\frac{\eta}{2}\right) + \frac{2}{\sqrt{\pi}}\left[1 - \exp\left(-\frac{\eta^2}{4}\right)\right], \quad \theta(0,\eta) = \text{erfc}\left[\frac{\eta}{2}\sqrt{\frac{3Pr}{3 + 4N_R}}\right],$$

(2.23)

$$\phi(0,\eta) = \text{erfc}\left[\frac{\sqrt{LeSc}\,\eta}{2}\right].$$

where the complementary error function erfc, is defined as;

$$\text{erfc}(\eta) = \frac{2}{\sqrt{\pi}}\int_{\eta}^{\infty} \exp\left(-t^2\right)dt.$$

3. Method of solution

The spectral perturbation method (SPM) is used for solving Eqs (2.14)-(2.16). In the spectral perturbation method, we generate series equations using the standard perturbation approach and then solve the series equations integrated in the space direction η numerically using the Chebyshev spectral collocation method. With the spectral methods, we can solve higher order perturbation equations easily. Following (Seshadri *et al.* [7]; Nazar *et al.* [8]), a series expansion is constructed to approximate $f(\xi,\eta)$, $\theta(\xi,\eta)$ and $\phi(\xi,\eta)$ solution by regarding ξ as a small parameter and looking for a perturbation approximation in the form

$$f(\xi,\eta) = \sum_{k=0}^{+\infty} \xi^k f_k(\eta)\ , \quad \theta(\xi,\eta) = \sum_{k=0}^{+\infty} \xi^k \theta_k(\eta)\ , \quad \phi(\xi,\eta) = \sum_{k=0}^{+\infty} \xi^k \phi_k(\eta)\ .$$

(3.1)

Substituting Eq. (3.1) into Eqs (2.14)-(2.16) together with the boundary conditions (2.17) and balancing terms of equal power of ξ, we obtain,

$$f_0''' + \frac{\eta}{2}f_0'' = 0, \quad f_0(0) = 0, \quad f_0'(0) = 1, \quad f_0'(\infty) = 0,$$

(3.2)

$$\left(1 + \frac{4N_R}{3}\right)\theta_0'' + Pr\frac{\eta}{2}\theta_0' = 0, \quad \theta_0(0) = 1, \quad \theta_0(\infty) = 0,$$

(3.3)

$$\phi_0'' + LeSc\frac{\eta}{2}\phi_0' = 0, \quad \phi_0(0) = 1, \quad \phi_0(\infty) = 0\ ,$$

(3.4)

$$f_k''' + \frac{\eta}{2} f_k'' - k f_k' = \frac{\eta}{2} f_{k-1}'' - (k-1) f_{k-1}' - \lambda \theta_{k-1} - \lambda N_b \phi_{k-1} +$$

$$+ \sum_{i=0}^{k-1} \left[f_{k-1-i}' f_i' - f_{k-1-i} f_i'' - \lambda \alpha \theta_{k-1-i} \theta_i - \lambda N_b \sigma \phi_{k-1-i} \phi_i \right], \tag{3.5}$$

$$f_k(0) = 0, \quad f_k'(0) = 0, \quad f_k'(\infty) = 0, \quad k \geq 1,$$

$$\left(1 + \frac{4 N_R}{3}\right) \theta_k'' + \frac{\eta}{2} \Pr \theta_k' - \Pr k \theta_k = \frac{\eta}{2} \Pr \theta_{k-1}' +$$

$$- \Pr(k-1) \theta_{k-1} - \mathrm{He}\, \theta_{k-1} - \sum_{i=0}^{k-1} \Pr \left[f_{k-1-i} \theta_i' \right], \tag{3.6}$$

$$\theta_k(0) = 0, \quad \theta_k(\infty) = 0, \quad k \geq 1,$$

$$\phi_k'' + \frac{\eta}{2} \mathrm{LeSc}\, \phi_k' - \mathrm{LeSc}\, k \phi_k = \frac{\eta}{2} \mathrm{LeSc}\, \phi_{k-1}' +$$

$$- \mathrm{LeSc}(k-1) \phi_{k-1} - \sum_{i=0}^{k-1} \mathrm{LeSc} \left[f_{k-1-i} \phi_i' \right], \tag{3.7}$$

$$\phi_k(0) = 0, \quad \phi_k(\infty) = 0, \quad k \geq 1.$$

The Chebyshev spectral collocation method is applied to integrate Eqs (3.5)-(3.7). The spectral method is based on the Chebyshev polynomials defined on the domain $[-1,1]$ by

$$T_l(x) = \cos \left[l \cos^{-1}(x) \right]. \tag{3.8}$$

Before implementing the spectral method, we first transform the physical domain on which the governing equation is defined to the region $[-1,1]$ where the spectral method can then be applied. This can be done with the aid of the domain truncation procedure, the problem is solved in the interval $[0,L]$ in place of $[0,\infty)$, where L is the scaling parameter taken to be large. This leads to the transformation

$$x = \frac{2\eta}{L} - 1, \quad -1 \leq x \leq 1. \tag{3.9}$$

The Gauss-Lobatto collocation points [20-22] are used to define the Chebyshev nodes $[-1,1]$ described as

$$xj = \cos \left(\frac{\pi j}{N_x} \right), \quad -1 \leq x \leq 1, \quad j = 0, 1, 2 \ldots, N_x \tag{3.10}$$

where ($N_x + 1$) is the total number of collocation points.

The fundamental aim following the spectral collocation method is the introduction of a differential

matrix D. The differential matrix D used to approximate the derivatives of the unknown variables $f_k(\eta), \theta_k(\eta), \phi_k(\eta)$ at the collocation points can be defined as

$$\left.\frac{df_k}{d\eta}\right|_{\eta=\eta_j} = \sum_{l=0}^{N_x} D_{jl} f_k(x_l) = DF_k, \qquad j=0,1,...,N_x,$$

$$\left.\frac{d\theta_k}{d\eta}\right|_{\eta=\eta_j} = \sum_{l=0}^{N_x} D_{jl} \theta_k(x_l) = D\Theta_k, \qquad j=0,1,...,N_x, \tag{3.11}$$

$$\left.\frac{d\phi_k}{d\eta}\right|_{\eta=\eta_j} = \sum_{l=0}^{N_x} D_{jl} \phi_k(x_l) = D\Phi_k, \qquad j=0,1,...,N_x$$

where (N_x+1) is the number of collocation points, $D=2D/L$, and

$$F_k = \left[f_k(x_0), f_k(x_1),...,f_k(x_{N_x}) \right]^T, \qquad \Theta_k = \left[\theta_k(x_0), \theta_k(x_1),...,\theta_k(x_{N_x}) \right]^T,$$

$$\Phi_k = \left[\phi_k(x_0), \phi_k(x_1),...,\phi_k(x_{N_x}) \right]^T, \tag{3.12}$$

is the vector function at the collocation points. We obtain the higher order derivatives as powers of D, that is

$$f_k^{(p)} = D^p F_k, \qquad \theta_k^{(p)} = D^p \Theta_k, \qquad \phi_k^{(p)} = D^p \Phi_k, \tag{3.13}$$

where p is the order of the derivatives. The matrix D is of size $(N_x+1)\times(N_x+1)$ and its entries are defined in [22] as

$$D_{jl} = \frac{c_j}{c_l} \frac{(-1)^{j+l}}{\tau_j - \tau_l} \quad j \neq l; \quad j,l = 0,1,2,N, \quad D_{ll} = -\frac{\tau_l}{2(1-\tau_l^2)} \quad 1 \le j = l \le N-1,$$

$$D_{00} = \frac{2N^2+1}{6} = -D_{N_x N_x}, \tag{3.14}$$

with

$$c_l = \begin{cases} 2, & l = 0, N_x \\ -1, & -1 \le l \le N_x - 1. \end{cases} \tag{3.15}$$

Substituting Eqs (3.11)-(3.14) into Eqs (3.5)-(3.7) gives

$$A_{1,k-1} F_k = B_{1,k-1}, \tag{3.16}$$

$$A_{2,k-1} \Theta_k = B_{2,k-1}, \tag{3.17}$$

$$A_{3,k-1}\mathbf{\Phi}_k = B_{3,k-1},$$ (3.18)

subject to the following boundary conditions

$$\sum_{l=0}^{N_x} D_{0l} f_k(x_l) = 0, \qquad \sum_{l=0}^{N_x} D_{N_x l} f_k(x_l) = 0, \qquad f_k(x_{N_x}) = 0,$$ (3.19)

$$\theta_k(x_{N_x}) = 0, \qquad \theta_k(x_0) = 0,$$ (3.20)

$$\phi_k(x_{N_x}) = 0, \qquad \phi_k(x_0) = 0$$ (3.21)

where $A_{1,k-1}$, $A_{2,k-1}$, $A_{3,k-1}$, $B_{1,k-1}$, $B_{2,k-1}$ and $B_{3,k-1}$ are defined as

$$A_{1,k-1} = D^3 + \text{diag}\left(\frac{\eta}{2}\right)D^2 - kD,$$

$$A_{2,k-1} = \text{diag}\left(1 + \frac{4N_R}{3}\right)D^2 + \text{diag}\left(\frac{\eta}{2}\Pr\right)D - k\Pr I,$$

$$A_{3,k-1} = D^2 + \text{diag}\left(\frac{\eta}{2}\text{LeSc}\right)D - k\,\text{LeSc}\,I,$$

(3.22)

$$B_{1,k-1} = \frac{\eta}{2}\left(D^2 F_{k-1}\right) - (k-1)DF_{k-1} - \lambda\mathbf{\Theta}_{k-1} - \lambda N_b\mathbf{\Phi}_{k-1} + \text{Sum}F,$$

$$B_{2,k-1} = \frac{\eta}{2}\Pr\left(D\mathbf{\Theta}_{k-1}\right) - \Pr(k-1)\mathbf{\Theta}_{k-1} - \text{Sum}\Theta,$$

$$B_{3,k-1} = \frac{\eta}{2}\text{LeSc}\left(D\mathbf{\Phi}_{k-1}\right) - \text{LeSc}(k-1)\mathbf{\Phi}_{k-1} - \text{Sum}\Phi$$

where $\boldsymbol{\eta} = \left[\eta_0, \eta_1, \cdots \eta_{N_x},\right]$, $\text{Sum}F$, $\text{Sum}\Theta$ and $\text{Sum}\Phi$ are defined as

$$\text{Sum}F = \sum_{i=0}^{k-1}\left[\left(DF_{k-1-i}\right)\left(DF_i\right) - F_{k-1-i}\left(D^2 F_i\right) - \lambda\alpha\theta_{k-1-i}\theta_i - \lambda N_b\sigma\phi_{k-1-i}\phi_i\right],$$

$$\text{Sum}\Theta = -\Pr\sum_{i=0}^{k-1}\left[F_{k-1-i}\left(D\mathbf{\Theta}_i\right)\right], \quad \text{Sum}\Phi = -LeSc\sum_{i=0}^{k-1}\left[F_{k-1-i}\left(D\mathbf{\Phi}_i\right)\right],$$

with I representing an $(N_x + 1)\times(N_x + 1)$ identity matrix and diag() is a diagonal matrix obtained from the vector $\left(x_0, x_1, ..., x_{N_x},\right)$. The boundary conditions Eq.(3.19) are imposed on the first, $N_x th$ row (second from

the last row) and $(N_x + 1)$ st row (last row) rows and first and last columns of Eq. (3.16) to obtain

$$
\begin{bmatrix}
D_{0,0} & D_{0,1} & \cdots & & \cdots & D_{0,N_x-1} & D_{0,N_x} \\
& & & A_{1,k-1} & & & \\
D_{N_x,0} & D_{N_x,1} & \cdots & & \cdots & D_{N_x,N_x-1} & D_{N_x,N_x} \\
0 & 0 & \cdots & & \cdots & 0 & 1
\end{bmatrix}
\begin{bmatrix}
f_k(x_0) \\
f_k(x_1) \\
\vdots \\
\vdots \\
f_k(x_{N_x-1}) \\
f_k(x_{N_x})
\end{bmatrix}
=
\begin{bmatrix}
0 \\
B_{1,k-1}(x_1) \\
\vdots \\
B_{1,k-1}(x_{N_x-1}) \\
0 \\
0
\end{bmatrix}
\tag{3.22}
$$

while the boundary conditions Eqs (3.20) and (3.21) are imposed on the first and last rows and columns of Eqs (3.17) and (3.18) respectively to obtain

$$
\begin{bmatrix}
1 & 0 & \cdots & & \cdots & 0 & 0 \\
& & & A_{2,k-1} & & & \\
0 & 0 & \cdots & & \cdots & 0 & 1
\end{bmatrix}
\begin{bmatrix}
\theta_k(x_0) \\
\theta_k(x_1) \\
\vdots \\
\vdots \\
\theta_k(x_{N_x})
\end{bmatrix}
=
\begin{bmatrix}
0 \\
B_{2,k-1}(x_1) \\
\vdots \\
B_{2,k-1}(x_{N_x-1}) \\
0
\end{bmatrix}
\tag{3.23}
$$

and

$$
\begin{bmatrix}
1 & 0 & \cdots & & \cdots & 0 & 0 \\
& & & A_{3,k-1} & & & \\
0 & 0 & \cdots & & \cdots & 0 & 1
\end{bmatrix}
\begin{bmatrix}
\phi_k(x_0) \\
\phi_k(x_1) \\
\vdots \\
\vdots \\
\phi_k(x_{N_x})
\end{bmatrix}
=
\begin{bmatrix}
0 \\
B_{3,k-1}(x_1) \\
\vdots \\
B_{3,k-1}(x_{N_x-1}) \\
0
\end{bmatrix}.
\tag{3.24}
$$

Hence, starting from a known F_0, Θ_0, Φ_0, the solutions F_k, Θ_k, Φ_k, $k \geq 1$ can be obtained from Eqs (3.22)-(3.24) as

$$
F_k = A_{1,k-1}^{-1} B_{1,k-1},
\tag{3.25}
$$

$$
\boldsymbol{\Theta}_k = A_{2,k-1}^{-1} B_{3,k-1},
\tag{3.26}
$$

$$
\boldsymbol{\Phi}_k = A_{3,k-1}^{-1} B_{4,k-1}.
\tag{3.27}
$$

3. Results and discussion

In this section, the nonlinear partial differential equations (2.14)-(2.16), together with the boundary conditions (2.17) were solved using the spectral perturbation method (SPM). The approximate numerical solutions of the skin friction coefficients, surface heat transfer, and the surface mass transfer rate at different values of the flow parameters were presented. Graphical results for velocity, temperature, and concentration profiles for different values of the physical parameter significant to the flow were also presented. The SPM series was used to generate results from the initial analytical solution at up to results close to the steady-state values. In order to ascertain the accuracy of our method, results generated using the SPM were compared with published work of [12], and an excellent agreement was attained between the SPM and the work of [12]. The results presented in this study were generated, through numerical experimentation which was found to give accurate results. The number of collocation points used in the spectral method discretization was the same, for both methods. We note that the values of all physical parameters used in this study were chosen based on the values used in the literature related to this work.

Table 1 displays the approximate numerical solutions of the skin friction coefficient and the reduced Nusselt and Sherwood numbers at different values of ξ. The table further shows a comparison of the SPM and the published work of [12]. From the table, it can be seen that the SPM results match perfectly well with those of [12] up to six decimal digits. In addition, the numerical results from the table show an increase of $f''(\xi,0)$, $-\theta(\xi,0)$, and $-\phi(\xi,0)$ with increasing values of ξ.

In Table 2, an excellent agreement between the SPM and the approximate numerical solutions obtained by [12] for $f''(\xi,0)$, $-\theta(\xi,0)$ and $-\phi(\xi,0)$ is observed for selected physical parameters. It can be seen from the table that the SPM and the SRM numerical results match entirely well up to six decimal places. We also observe from the table that for increased values of N_b, λ, σ and α, there is an increase in the skin friction coefficient, Nusselt number and Sherwood number.

Table 1. Comparison of SPM approximate solutions for $f''(0,\xi)$, $-\theta'(0,\xi)$, and $-\phi'(0,\xi)$ against those of Ref. [12] for different values of ξ when $L=30$, $N_x=100$, $\lambda=0.5$, $Pr=0.7$, $Le=3$, $Sc=1$, $\alpha=1$, $\sigma=1$, $He=0$, and $N_R=0$.

ξ	$f''(\xi,0)$		$-\theta'(\xi,0)()$		$-\phi'(\xi,0)$	
	SPM	Ref. [12]	SPM	Ref. [12]	SPM	Ref. [12]
0.1	*-0.540183*	*-0.540183*	*0.475790*	*0.475790*	*0.993124*	*0.993124*
0.2	*-0.516888*	*-0.516888*	*0.479891*	*0.479891*	*1.010491*	*1.010491*
0.3	*-0.494398*	*-0.494398*	*0.484385*	*0.484385*	*1.029550*	*1.029550*
0.4	*-0.472821*	*-0.472821*	*0.489330*	*0.489330*	*1.050616*	*1.050616*
0.5	*-0.452295*	*-0.452295*	*0.494804*	*0.494804*	*1.074110*	*1.074110*
0.6	*-0.432994*	*-0.432994*	*0.500905*	*0.500905*	*1.100615*	*1.100615*
0.7	*-0.415145*	*-0.415145*	*0.507775*	*0.507775*	*1.130989*	*1.130989*
0.8	*-0.399066*	*-0.399066*	*0.515629*	*0.515629*	*1.166621*	*1.166621*
0.9	*-0.385221*	*-0.385221*	*0.524843*	*0.524843*	*1.268622*	*1.268622*

Table 2. Variation of the SPM approximate solutions of $f''(0,\xi)$, $-\theta'(0,\xi)$, and $-\phi'(0,\xi)$ against those of Ref. [12] for different values of λ, α, N_R, σ when $\xi = 0.5$, $L = 30$, $N_x = 100$, $Pr = 0.7$, $Le = 3$, $Sc = 1$, $He = 0$, $N_R = 0$.

λ	α	N_b	σ	$f''(\xi,0)$		$-\theta'(\xi,0)$		$-\phi'(\xi,0)$	
				SPM	Ref. [12]	SPM	Ref. [12]	SPM	Ref. [12]
0.1	1	0.5	1	-0.721619	-0.721619	0.488512	0.488512	1.063098	1.063098
0.5	1	0.5	1	-0.452295	-0.452295	0.494804	0.494804	1.074110	1.074110
1.0	1	0.5	1	-0.123169	-0.123169	0.502489	0.502489	1.0878165	1.087615
0.5	0.1	0.5	1	-0.549445	-0.549445	0.492700	0.492700	1.070271	1.070271
0.5	0.5	0.5	1	-0.506182	-0.506182	0.493637	0.493637	1.071980	1.071980
0.5	1	0.5	1	-0.452295	-0.452295	0.494804	0.494804	1.074110	1.074110
0.5	1	0.1	1	-0.516058	-0.516058	0.493757	0.493757	1.071997	1.071997
0.5	1	0.5	1	-0.452295	-0.452295	0.494804	0.494804	1.074110	1.074110
0.5	1	1	1	-0.372924	-0.372924	0.496105	0.496105	1.076742	1.076742
0.5	1	0.5	0.1	-0.481198	-0.481198	0.494428	0.494428	1.073293	1.073293
0.5	1	0.5	0.5	-0.468347	-0.468347	0.494595	0.494595	1.073656	1.073656
0.5	1	0.5	1	-0.452295	-0.452295	0.494804	0.494804	1.074110	1.074110
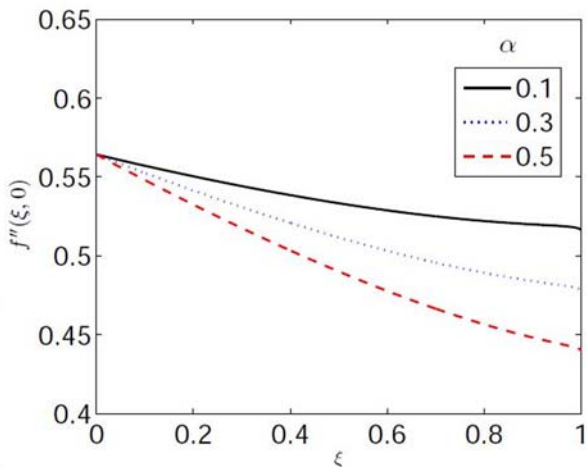
Fig.1. Effect of α on the skin friction coefficient $f''(\xi,\eta)$ for different ξ, with $N_x = 60$, $L = 20$, $\sigma = 1$, $N_R = 1$, $N_b = 0.5$, $\lambda = 0.5$.
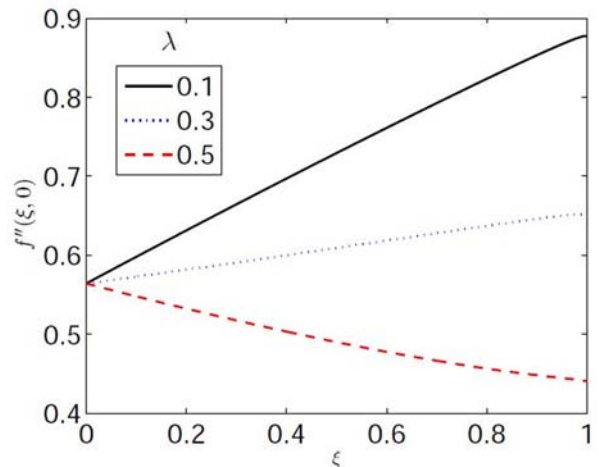
Fig.2. Effect of λ on the skin friction coefficient $f''(\xi,0)$ for different ξ, with $N_x = 60$, $L = 20$, $\sigma = 1$, $N_R = 1$, $N_b = 0.5$, $\alpha = 1$.

Figure 1 depicts the effect of α on the skin friction $f''(\xi,0)$. It can be seen that the skin friction decreases with an increase in the values of α. Figure 2 shows the variation of the skin friction $f''(\xi,0)$ with λ. It can be observed from the figure that for values of $\lambda = 0.1$ and $\lambda = 0.3$, the skin friction increases while for $\lambda = 0.5$, the skin friction decreases. This implies that the skin friction is an increasing function of ξ for $\lambda = 0.1$ and $\lambda = 0.3$, and a decreasing function of ξ for $\lambda = 0.5$. Figures 3 and 4 present the effect of σ and N_b, respectively, on the skin friction coefficient. It can be seen that for all the values of σ and N_b, the skin

friction is observed to be decreasing. A further increase in the values of He and N_R, decreases the skin friction coefficient, the more as seen in Figures 5 and 6.
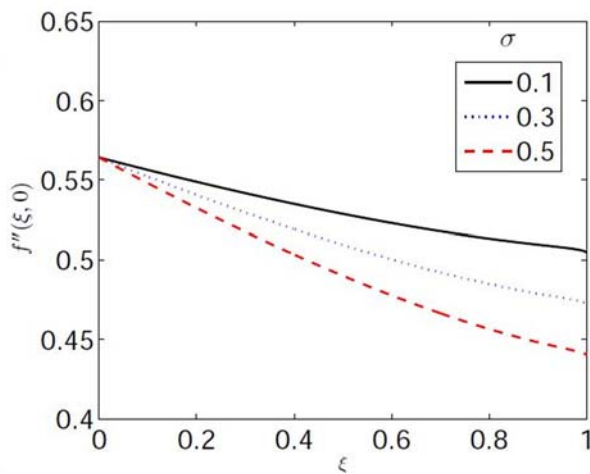
Fig.3. Effect of σ on the skin friction coefficient $f''(\xi,0)$ for different ξ, with $N_x = 60$, $L = 20$, $N_R = 1$, $N_b = 0.5$, $\alpha = 1$, $\lambda = 0.5$.
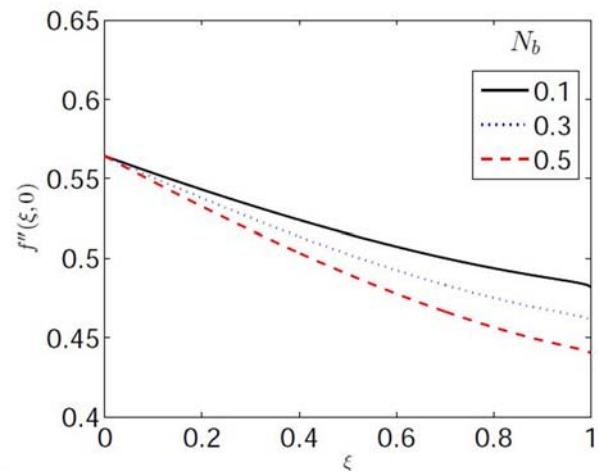
Fig.4. Effect of N_b on the skin friction coefficient $f''(\xi,\eta)$ for different ξ, with $N_x = 60$, $L = 20$, $\sigma = 1$, $N_R = 1$, $\alpha = 1$, $\lambda = 0.5$.
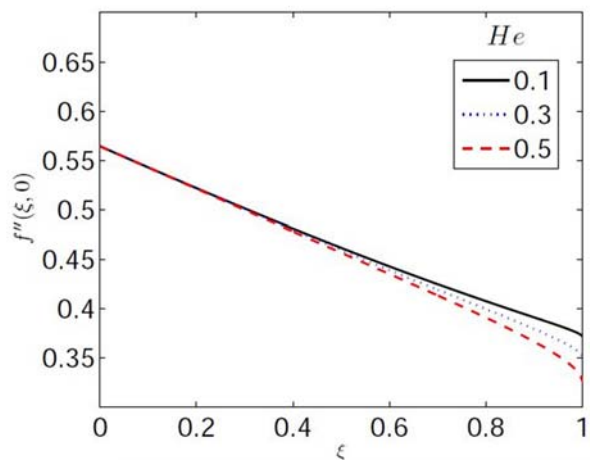
Fig.5. Effect of He on the skin friction coefficient $f''(\xi,0)$ for different ξ, with $N_x = 60$, $L = 20$, $\sigma = 1$, $N_R = 1$, $N_b = 0.5$, $\alpha = 1$, $\lambda = 0.5$.
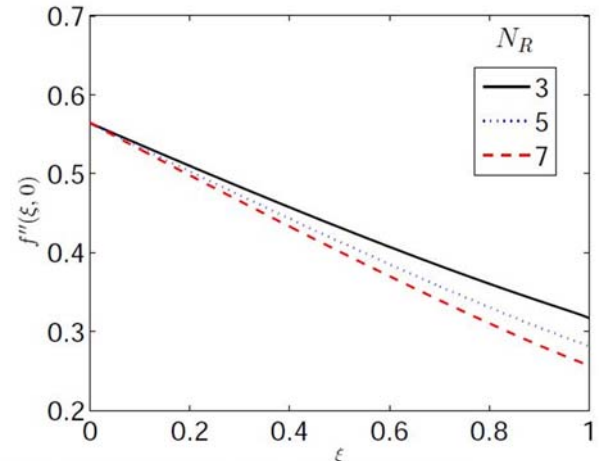
Fig.6. Effect of N_R on the velocity profile $f''(\xi,0)$ with $N_x = 60$, $L = 20$, $\xi = 0.5$, $\sigma = 1$, $N_b = 0.5$, $\alpha = 1$, $\lambda = 0.5$.

The effect of the heat generation parameter He on the temperature profile is displayed in Fig.7. As would be expected, the temperature profile is enhanced by increasing He. In physical terms, He enhances fluid temperature, leading to an increase in the thermal boundary layer thickness. In Fig. 8, we present the solution of temperature profile for various values of N_R. Increasing the values of N_R decreases the temperature profile which leads to a decrease in the thermal boundary layer thickness. Figure 9 shows the impact of Pr on the temperature profile. We note that an increase in Pr causes the temperature profile to

decrease. As we know, Pr is the ratio of viscosity to diffusivity, and thus gives an insight into the physics of the fluid. Increasing Pr decelerates the temperature profiles so that the thermal boundary layer thickness becomes thinner. The reduction is due to the increase in the viscosity, which in turn enhances the momentum boundary layer thickness. The behavior of Pr on the temperature profile $\theta(\xi,\eta)$ correlates with results earlier obtained by Awad *et al*. [12]. Figure 10 depicts the effect of Sc on the concentration profile ($\phi(\xi,\eta)$). It can be seen from the figure that as *Sc* increases, the concentration profile and the boundary layer thickness decreases. This implies that an increase in the Schmidt number corresponds to a reduction in the concentration profile. Figure 11 shows the effect of various values of Le on the concentration profile. It can be observed that an increase in the Lewis number decreases the concentration profile as well as the concentration boundary layer thickness.
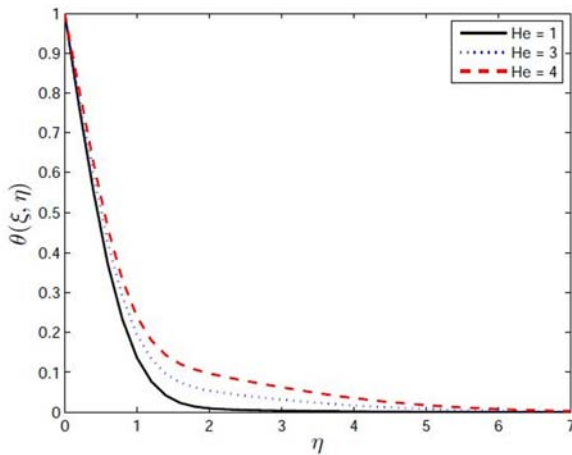
Fig.7. Effect of He on the temperature profile $\theta(\xi,\eta)$, with $N_R=1$, $N_x=60$, $L=20$, $\xi=0.5$, He$=1$, Pr$=0.7$, $\alpha=1$, $\lambda=0.5$.
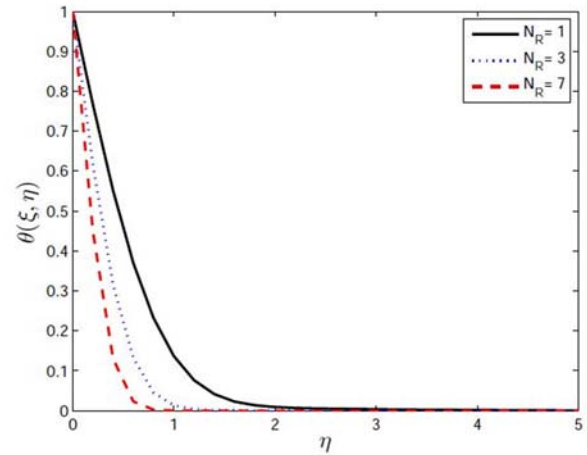
Fig.8. Effect of N_R on the temperature profile $\theta(\xi,\eta)$, with He$=1$, $N_x=60$, $L=20$, $\xi=0.5$, He$=1$, Pr$=0.7$, $\alpha=1$, $\lambda=0.5$.
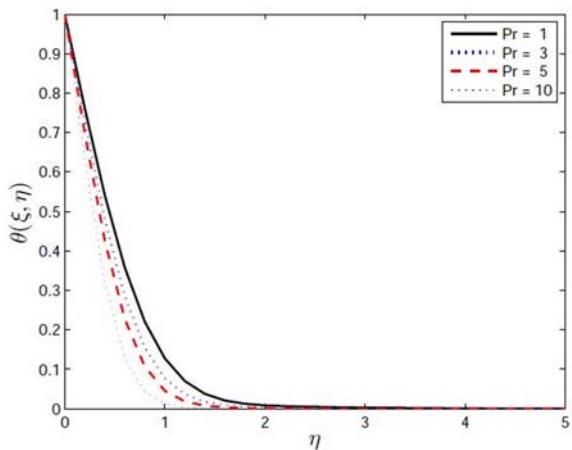
Fig.9. Effect of Pr on the temperature profile $\theta(\xi,\eta)$, with $N_x=60$, $L=20$, $\xi=0.5$, He$=1$, $N_R=1$, $\alpha=1$, $\lambda=0.5$.
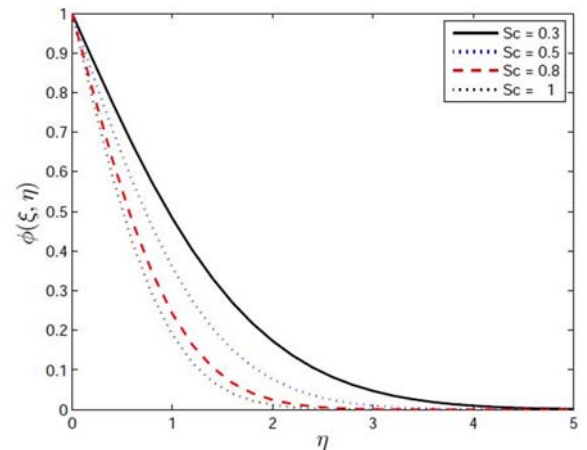
Fig.10. Effect of Sc on the concentration profile $\phi(\xi,\eta)$ with $N_x=60$, $L=20$, $\xi=0.5$, Le$=1$, $N_b=0.5$, $\sigma=1$, $\lambda=0.5$.
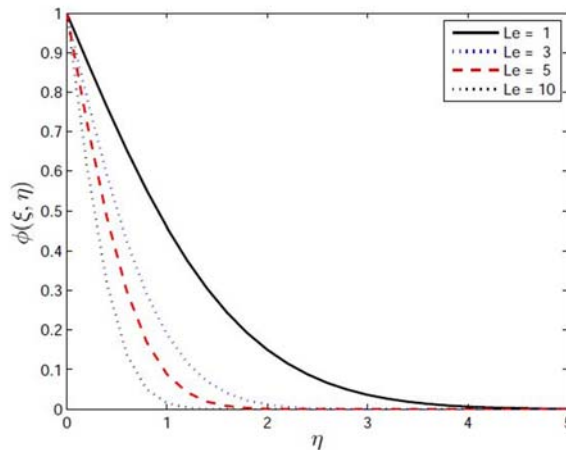
Fig.11. Effect of Le on the concentration profile $\phi(\xi,\eta)$ with, $N_x = 60$, $L = 20$, $\xi = 0.5$, $\text{Sc} = 1$, $N_b = 0.5$, $\sigma = 1$, $\lambda = 0.5$.

4. Conclusions

In this study, we have discussed the application of the SPM on systems of nonlinear PDEs. The SPM was used to solve the unsteady nonlinear MHD flow in the presence of thermal radiation and heat generation. The flow model investigated the effects of the embedded parameters in detail. Approximate numerical solutions of the skin friction coefficient, surface heat, and mass transfer rate were generated using the SPM at different flow parameter values and dimensionless time values. The SPM results were validated with results from the literature, where an excellent agreement between the two sets of results was achieved. The graphical results obtained were also found to agree with those found in similar studies in the literature. With the SPM, higher-order approximate solutions are obtainable, where not possible, or very difficult to find with the usual perturbation schemes. For problems similar to the one investigated in this investigation, the SPM can be used efficiently even for complicated expansions, which cannot be solved analytically beyond the first-order approximation. In as much as the SPM is limited to problems with small parameters, accurate numerical solutions can be obtained as compared to the ordinary perturbation schemes. The numerical results presented in the study indicate that the SPM can be used to solve complex nonlinear systems of PDEs, mainly those defined using the transformation of [17].

Nomenclature

C_p – specific heat at constant pressure of the fluid

D – mass diffusivity

g – acceleration due to gravity

He – heat generation parameter

K_0 – fluid thermal conductivity ratio

Le – Lewis number

MHD – magnetohydrodynamic

N_b – buoyancy parameter

N_R – thermal radiation parameter

Pe_x – Peclet number

Pr – Prandtl number

Q_0 – heat generation constant

Sc – Schmidt number

u, v – velocity Components

α_m – thermal diffusivity

β_0, β_1 – thermal expansion coefficients

β_2, β_3 – solutal expansion coefficients

γ – nonlinear temperature parameter

ν – kinematic viscosity

ρ – fluid density

σ – fluid electrical conductivity

ψ – stream function

Acknoledgement

References

[1] Hayat T., Qasim M. and Abbas Z. (2010): *Homotopy solution for the unsteady three dimensional MHD flow and mass transfer in a porous space.*– Communications in Nonlinear Science and Numer. Simu., vol.15, No.9, pp.2375-2387.

[2] Kumari M. and Nath G. (2009): *Analytical solution of unsteady three-dimensional MHD boundary layer flow and heat transfer due to impulsively stretched plane surface.*– Communications in Nonlinear Science and Numer. Simu., vol.14, No.8, pp.3339-3350.

[3] Takhar H.S., Chamkha A.J. and Nath G. (2001): *Unsteady three-dimensional MHD boundary-layer flow due to the impulsive motion of a stretching surface.*– Acta Mechanica, vol.146, No.1-2, pp.59-71.

[4] Olanrewaju P.O., Olanrewaju M.A. and Ajadi D.A. (2012): *Unsteady three dimensional MHD flow and mass transfer in a porous space in the presence of thermal radiation.*– Int. Research J. of Petroleum and Gas Exploration Research, vol.2. No.2, pp.044-051.

[5] Makinde O.D., Olanrewaju P.O. and Charles M.W. (2011): *Unsteady convection with chemical reaction and radiative heat transfer past a flat porous plate moving through a binary mixture.*– Afrika Matematika, vol.22, No.1, pp.65-78.

[6] Abbas Z., Hayat T., Pop I. and Ashgar S. (2010): *Effects of radiation and magnetic field on the mixed convection stagnation-point flow over a vertical stretching sheet in a porous medium.*– Int. J. of Heat and Mass Transfer, vol.53, No.1, pp.466-474.

[7] Seshadri R., Sreeshylan N. and Nath G. (2002): *Unsteady mixed convection flow in the stagnation region of a heated vertical plate due to impulsive motion.*– Int. J. of Heat and Mass Transfer, vol.45, No.6, pp.1345-1352.

[8] Nazar R., Amin N. and Pop I. (2004): *Unsteady boundary layer flow due to a stretching surface in a rotating fluid.*– Mechanics Research Commu., vol.31, No.1, pp.121-128.

[9] Liao S. (2006): *An analytic solution of unsteady boundary-layer flows caused by an impulsively stretching plate.*– Communications in Nonlinear Sci. and Num. Simulation, vol.11, No.3, pp.326-339.

[10] Mehmood A., Ali A., Takhar H.S. and Shah T. (2008): *Unsteady three-dimensional MHD boundary-layer flow due to the impulsive motion of a stretching surface.*– Journal of Applied Fluid Mech., vol.199, No.1-4, pp.241-249.

[11] Xu H., Liao S. and Pop I. (2007): *Series solutions of unsteady three-dimensional MHD flow and heat transfer in the boundary layer over an impulsively stretching plate.*– European J. of Mech.-B/Fluids, vol.26, No.1, pp.15-27.

[12] Awad F.G., Motsa S.S. Makukula Z.G. and Sibanda P. (2014): *The Spectral Homotopy Analysis Method Extended to Systems of Partial Differential Equations.*– Abstract and Applied Analysis, vol.2014, Article ID 241594, 11 pages, doi:10.1155/2014/241594.

[13] Agbaje T.M. and Motsa S.S. (2015): *Comparison between spectral perturbation and spectral relaxation approach for unsteady heat and mass transfer by MHD mixed convection ow over an impulsively stretched vertical surface with chemical reaction effect*.– Journal of Interpolation and Approximation in Scientific Computing, vol.2015, No.1, pp.48-83.

[14] Motsa S.S. (2015): *On Efficient Spectral Perturbation Method for Unsteady Boundary-Layer Flows Caused by an Impulsively Stretching Plate*.– Journal of Applied Fluid Mechanics, vol. 9, No. 2, pp. 999-1011.

[15] Agbaje T.M., Motsa S.S, Mondal S. and Sibanda P. (2017): *A large parameter spectral perturbation method for nonlinear systems of partial differential equations that models boundary layer flow problems*. – Frontiers in Heat and Mass Transfer, vol. 9, No.1, pp.1-13.

[16] Agbaje T.M., Mondal S., Makukula Z.G., Motsa S.S. and Sibanda P. (2018): *A new numerical approach to MHD stagnation point flow and heat transfer towards a stretching sheet*. – Ain Shams Engineering Journal, vol.9, No.2, pp.233-243.

[17] Williams J.C. and Rhyne T.B. (1980): *Boundary layer development on a wedge impulsively set into motion*.– SIAM J. on App. Math., vol.38, No.2, pp.215-224.

[18] Karcher C. and Müller U. (1994): *Bénard convection in a binary mixture with a nonlinear density-temperature relation*.– Physical Review E, vol.49, No.5, pp.4031-4043.

[19] Partha M.K. (2010): *Nonlinear convection in a non-Darcy porous medium*.– Applied Math. and Mech., vol.31, No.5, pp.565-574.

[20] Don W.S. (1995): *Accuracy and speed in computing the Chebyshev collocation derivative*.– SIAM J. on Scientific Comp., vol.16, No.6, pp.1253-1268.

[21] Hussaini M.Y. and Zang T.A. (1987): *Spectral methods in fluid dynamics*.– Annual Review of Fluid Mechanics, vol.19, No.1, pp.339-367.

[22] Trefethen L.N. (2000): *Spectral Methods in MATLAB*.– SIAM, 1st Edition.